

# Hysteresis loops and adiabatic Landau-Zener-Stuckelberg transitions in the magnetic molecule $\text{fv}_6\text{g}$

I. Rousochatzakis,<sup>1</sup> Y. Ajiro,<sup>2,3</sup> H. Mitamura,<sup>4</sup> P. Kogerler,<sup>1</sup> and M. Luban<sup>1</sup>

<sup>1</sup>Ames Laboratory and Department of Physics and Astronomy, Iowa State University, Ames, Iowa, 50011

<sup>2</sup>Department of Chemistry, Graduate School of Science, Kyoto University, Kyoto 606-8502, Japan

<sup>3</sup>CREST, Japan Science and Technology Agency, Saitama 332-0012, Japan

<sup>4</sup>Institute for Solid State Physics, University of Tokyo, Chiba 106, Japan

We have observed hysteresis loops and abrupt magnetization steps in the magnetic molecule  $\text{fv}_6\text{g}$ , where each molecule comprises a pair of identical spin triangles, in the temperature range 1–5 K for external magnetic fields  $B$  with sweep rates of several Tesla/ms executing a variety of closed cycles. The hysteresis loops are accurately reproduced using a generalization of the Bloch equation based on direct one-phonon transitions between the instantaneous Zeeman-split levels of the ground state (an  $S = 1=2$  doublet) of each spin triangle. The magnetization steps occur for  $B = 0$  and they are explained in terms of adiabatic Landau-Zener-Stuckelberg transitions between the lowest magnetic energy levels as mediated by inter-triangle anisotropic exchange of order 0.4 K.

PACS numbers: 75.50.Xx, 75.45.+j, 71.70.-d

Magnetic molecules provide a very convenient platform for exploring fundamental issues in nanomagnetism. Heisenberg exchange between the magnetic-ion spins embedded in each molecule gives rise to a discrete spectrum of magnetic energy levels. Moreover, the magnetic interaction (dipole-dipole) between molecules is generally so small as compared to intra-molecular exchange interactions that a crystal sample may be regarded as a macroscopic assembly of independent identical quantum nanomagnets. One significant goal is to understand the interactions of the magnetic molecules with the environment ("heat bath"), for example via phonons. In particular, it is essential to understand the nature of the thermal relaxation mechanism, the controlling factors responsible for irreversible and dissipative phenomena, and the detailed route to thermal equilibrium of these nano-size quantum spin systems. The simpler the spin system the greater the prospects for achieving a deep understanding of the underlying issues, and this opportunity is provided by the magnetic molecule  $\text{fv}_6\text{g}$ [1]. Each  $\text{fv}_6\text{g}$  includes a pair of triangles of exchange-coupled vanadyl ( $\text{VO}^{2+}$ , spin 1/2) ions. As shown below, at low temperatures the instantaneous magnetization,  $M(t)$ , of this spin system, in response to pulsed magnetic fields,  $B(t)$ , with sweep rates of several Tesla/ms, exhibits pronounced hysteresis loops as well as abrupt magnetization steps that are due to Landau-Zener-Stuckelberg (LZS) transitions[2, 3] between lowest energy levels. By explaining the details of the dynamical magnetization one establishes both the low-temperature relaxation mechanism for the individual magnetic molecules as well as microscopic information concerning the lowest energy levels, not readily accessible. Indeed, our analysis suggests the existence in this magnetic molecule of an effective inter-triangle anisotropic exchange of order 0.4 K; otherwise Kramers' theorem [4, 5] would forbid the occurrence of LZS transitions.

There are several important differences between the present work and previous studies of  $M(t)$  in magnetic molecules in time-dependent magnetic fields. From our observation of hysteresis effects in  $\text{fv}_6\text{g}$  we conclude that the thermal relaxation time in this molecule is of order 0.1 ms. This is many orders of magnitude shorter than those reported for "single-molecule magnets" such as  $\text{Mn}_{12}\text{g}$ [6] and  $\text{Fe}_8\text{g}$ [7] where a large anisotropy energy barrier is responsible for relaxation times of order  $10^3 - 10^5$  sec. Also, we assume that the phonon bottleneck effect which typically occurs at low temperatures (e.g.  $T < 200$  mK for  $\text{fv}_{15}\text{As}_6\text{g}$ [8]) does not arise: For the temperatures of our experiment ( $T > 1.5$  K) the number of available resonant phonons per molecule is large so that they equilibrate independently from the spins (typical times  $\tau_{\text{ph}} < 10^{-6}$  s, much smaller than both the experimental time scale  $\tau_{\text{exp}} \sim 1$  ms and the relaxation times of the spins). Moreover, due to the high sweep rate of  $B(t)$  in our measurements, LZS transitions are consequential only in the immediate vicinity of  $B = 0$ . Away from  $B = 0$ , we use a generalization of the standard Bloch equation for  $M(t)$ , where the relaxation rate depends on the instantaneous  $B(t)$ . The excellent agreement obtained between theory and experiment allows us to identify the dominant mechanism for thermal relaxation in terms of direct one-phonon processes. To our knowledge, this is the first time that quantitative agreement between theory and experiment has been achieved for hysteresis loops in magnetic molecules.

We first summarize the most important known features of  $\text{fv}_6\text{g}$ [1]. The magnetic molecule  $[\text{H}_4\text{V}_6^{\text{IV}}\text{O}_8(\text{PO}_4)_4\text{f}(\text{OCH}_2)_3\text{CCH}_2\text{OHg}_2]^{6-}$ , abbreviated as  $\text{fv}_6\text{g}$ , and isolated as  $(\text{CN}_3\text{H}_6)_4\text{N}_2\text{fv}_6\text{g} \cdot 14\text{H}_2\text{O}$ , may be pictured (see Fig. 1) in terms of two identical triangular units per molecule, each unit consisting of three spins  $s = 1=2$  ( $\text{VO}^{2+}$  ions) interacting via isotropic antiferromagnetic (AFM) exchange. Two of the 2-spin exchange constants

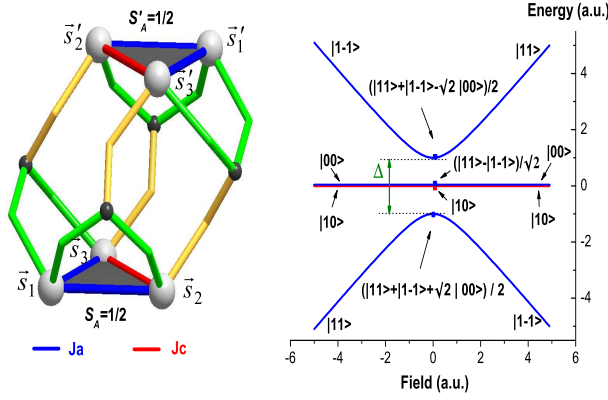


FIG. 1: Left: Structure of the two spin triangles in the  $Fv_6g$  anion (bright grey spheres). Phosphate exchange paths (green), and other ligands not shown, mediate strong intra-triangle exchange ( $J_a$ , blue) and weak inter-triangle exchange (yellow bonds). At low temperatures each triangle behaves as a spin  $1/2$  entity ( $S_A = S'_A = 1/2$ ). Right: Energy diagram for one scenario of inter-triangle exchange where a term of the form  $(-2)(S_{Ax}S_{Ax}^0 - S_{Az}S_{Ax}^0)$  admixes several of the states  $|11\rangle; S_A = 1/2; S'_A = 1/2\rangle, |10\rangle; S_A = 1/2; S'_A = 1/2\rangle$ , shown as blue lines.

(shown in blue) are equal ( $J_a \approx 65$  K in units of  $k_B$ ), and an order of magnitude larger than the third (shown in red,  $J_c \approx 7$  K). Additionally, from nuclear magnetic resonance (NMR) studies and chemical structure analysis it has been argued that there exists a very weak inter-triangle exchange interaction (yellow bonds, approximately 0.3 K). In the absence of inter-triangle exchange, for  $B = 0$  the ground state of each triangle consists of a 2-fold degenerate doublet with total spin  $S = 1/2$ , consistent with Kramers' theorem. The excited levels are a second degenerate doublet with  $S = 1/2$  and excitation energy ( $J_a - J_c \approx 58$  K), and a 4-fold degenerate level with  $S = 3/2$  and excitation energy (also measured from the ground state)  $3J_a \approx 97$  K. In the experiments described below we consider temperatures in the range 1.5–5 K and  $B < 25$  Tesla, well below the field value (74 Tesla) when the  $S = 3/2; M_S = 3/2$  level crosses the ground state  $S = 1/2; M_S = 1/2$  level. As such, it suffices to consider only the ground state doublet of each triangular unit. A weak residual inter-triangle anisotropic exchange will lift the 4-fold degeneracy for  $B = 0$  of each molecule and give rise (in general) to four distinct energy levels (see below). As remarked above, the occurrence of these splittings can be manifest when the molecules are subject to pulsed magnetic fields, giving rise to a sudden reversal in magnetization when the field crosses  $B = 0$ , as a result of LZS transitions between the split levels. Apart from the vicinity of  $B = 0$  the magnetic properties at low  $T$  of a  $Fv_6g$  sample may be accurately described in terms of an ensemble of inde-

pendent  $S = 1/2$  spin triangles.

In e-resolved magnetization measurements were performed on a powdered sample for half-cycle and full-cycle sweeps by a standard induction method using compensated pickup coils and a nondestructive long pulse magnet installed at ISSP. Utilizing fast digitizers, the inductive method provides data for  $dM/dt$  and  $dB/dt$  which are subsequently integrated to give results for  $M$  versus  $B$ . The pulsed fields have a nearly sinusoidal shape as a function of time, with a half-period about 21 ms (0–maximum–0). The sample of 36.9 mg was packed in a thin-walled cylindrical aluminum capsule (inner diameter 3.0 mm) and then directly immersed in a liquid Helium bath.

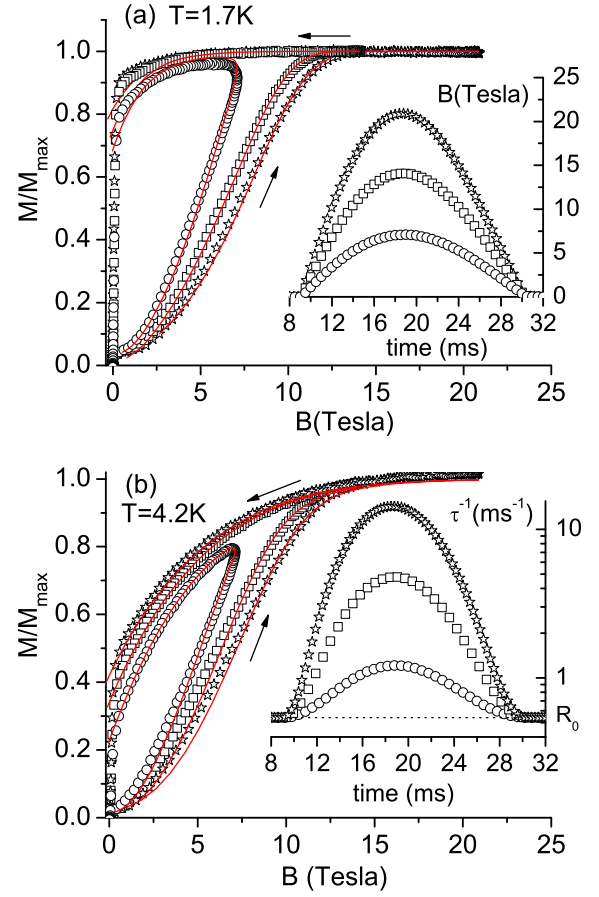


FIG. 2: Measured magnetization vs magnetic field for  $T = 1.7$  K (a) and  $T = 4.2$  K (b), for the three half-cycle sweeps shown in the inset of Fig. 2 (a). The solid red lines are obtained using Eqs. (1) and (2). The time dependence of the relaxation rate  $\tau^{-1}$  according to Eq. (2) for  $T = 4.2$  K is given in the inset of Fig. 2 (b). The dotted line indicates the residual constant  $R_0$  in Eq. (2). The sudden drop of  $M$  to zero at  $B = 0$  is explained in the text in the context of LZS transitions.

In Figs. 2 and 3 we present our experimental and theoretical results for the magnetization versus applied

magnetic field for two different temperatures (1.7 K and 4.2 K) and for half-cycle and full-cycle sweeps shown in the insets of Fig. 2 (a) and Figs. 3 (a) and 3 (b). The two striking features of the  $M$  vs.  $B$  data are hysteresis loops and the appearance of magnetization steps (in Fig. 2) and near-reversals (Fig. 3) in the immediate vicinity of  $B = 0$ . The hysteresis loops (all data except in the immediate vicinity of  $B = 0$ ) are reproduced (solid lines in Figs. 2 and 3) by numerical solution of the following generalization [10] of the familiar Bloch equation [4, 9]

$$\frac{d}{dt}M(t) = \frac{1}{(T; B(t))} [M_{eq}(T; B(t)) - M(t)]; \quad (1)$$

with the relaxation rate  $1 =$  given by

$$\frac{1}{(T; B(t))} = \frac{3(g_B)^3 V_{sl}^2}{2 v^5 h^4} B(t)^3 \coth\left[\frac{g_B B(t)}{2k_B T}\right] + R_0; \quad (2)$$

Here  $\mu_B$  is the Bohr magneton,  $\rho$  denotes the mass density,  $v$  the sound velocity,  $V_{sl}$  the characteristic modulation of the spin energy under long-wavelength acoustic deformation, and  $M_{eq}(T; B(t))$  is the standard two-level equilibrium magnetization for an instantaneous field  $B(t)$  and for temperature  $T$ , i.e.,  $M_{eq}(T; B(t)) = M_{max} \tanh[g_B B(t)/(2k_B T)]$ , where  $M_{max} = 2(N_A g_B \mu_B)$ . We have derived Eq. (1) from first principles [10] upon making the assumption that for these temperatures the phonons are in thermal equilibrium with the cryostat at all experimental times. The first term of Eq. (2) is the low-temperature relaxation rate of the spins due to direct one-phonon processes, where spin flips are triggered by an acoustic phonon mode meeting the resonance condition for the instantaneous energy separation of the two-level spin system. This term is a generalization of the standard expression for the relaxation rate due to one-phonon processes in a static external field [4]. Both the  $B(t)^3$  factor, proportional to the phonon energy density, and the statistical-mechanical factor depend on the instantaneous resonance frequency, proportional to  $B(t)$ . The numerical value of  $V_{sl}$  depends on the specific details of the spin-phonon coupling (see, for example, discussion for paramagnetic spins in Ref. [4]), which at present is unclear. The quantity  $R_0$  in Eq. (2) represents additional relaxation processes present and it is taken as a fitting parameter. Using the measured value of  $\rho = 1.93 \text{ g/cm}^3$  and estimating  $v = 3000 \text{ m/s}$ , we obtain excellent agreement with our data for the choices  $R_0 = 0.2 \text{ ms}^{-1}$  for  $T = 1.7 \text{ K}$  and  $R_0 = 0.5 \text{ ms}^{-1}$  for  $T = 4.2 \text{ K}$  and  $V_{sl} = k_B = 0.35 \text{ K}$ . Despite the smallness of  $R_0$  it is important to retain this term in order to achieve a good fit to the experimental data in the low-field regime (below 4 Tesla for 1.7 K and below 7 Tesla for  $T = 4.2 \text{ K}$ ); for higher fields the dominant contribution to  $1 =$  comes from the one-phonon term. We emphasize that the solution of Eq. (1) is extremely sensitive to the explicit functional form of the first term of Eq.

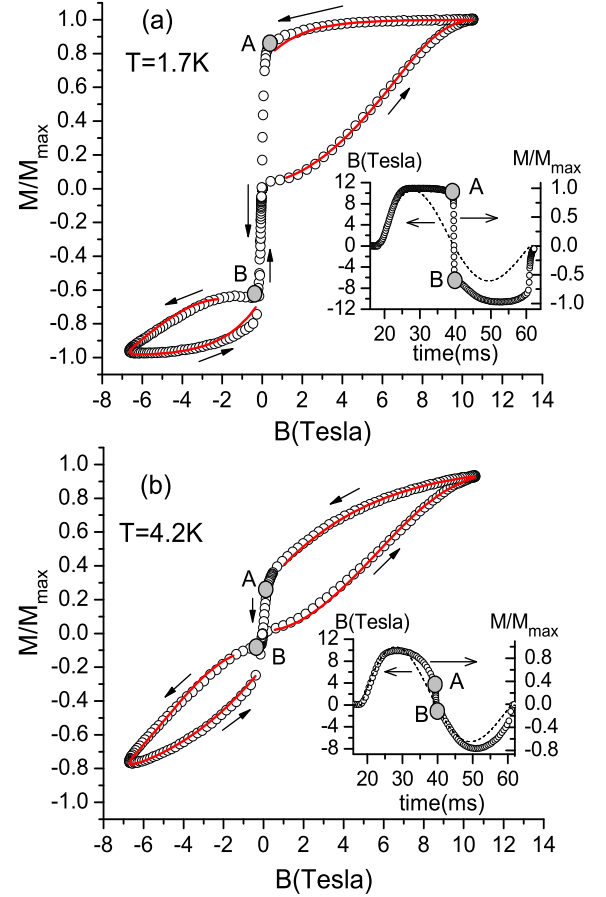


FIG. 3: Measured magnetization vs magnetic field for  $T = 1.7 \text{ K}$  (a) and  $T = 4.2 \text{ K}$  (b), for the full-cycle sweep shown in the inset of Figs. 3 (a) and 3 (b) (dotted lines). The solid lines are obtained using Eqs. (1) and (2). The insets also show the measured magnetization (circles) vs time. The LZS transitions occur in the interval between the points A and B.

(2)): Adopting a different choice of functional form one cannot achieve quantitative agreement with the observed hysteresis loops, for the whole field range and for different choices of field sweeps. Achieving an excellent fit to our measured data for a variety of choices of  $B(t)$  thus confirms the basic correctness of these two equations.

We now discuss the magnetization steps observed for  $B = 0$ , and in particular the interval between points A and B in Figs. 3 (a) and 3 (b) (the other steps seen in Figs. 2 and 3 have the same physical origin and will not be discussed separately). In this interval the external field varies approximately linearly with time, with sweep rates of order 1 Tesla/m.s. We note that at point A,  $M_A = M_{max}$  is somewhat less than unity due to thermal relaxation before entering the fast-reversal regime. Equivalently, at point A we are dealing with a statistical mixture of spin-up and spin-down states. The most

striking feature though is that the magnetization  $M_B$ , at point B, nearly equals  $M_A$ . We find that the time-widths of the near-reversals is shorter the faster the sweep rate, and is in the range 0.5–0.8 ms. We propose that adiabatic LZS transitions are responsible for the magnetization steps observed in our system. The characteristic energy gap of the LZS 2-level [13] model is related to the time-width  $t_{LZS}$  of the magnetization step and the field sweep rate  $r$  by the relation  $t_{LZS} = 2/(g_B r)$  [2, 3]. Thus, the measured time-widths of the steps give, as a first estimate for the zero-field energy gap, 0.4 K. Using the above estimate for  $\Delta$ , we are indeed in the regime of adiabatic LZS transitions, since the transition probability  $P_{LZS} = 1 - \exp(-\Delta^2/(2\hbar g_B r)) \approx 1$  [2, 3], thus implying that  $M_B = M_A$ . The observed deviation of  $M = M_{max}$  from exact reversal is about 15% for  $T = 1.7$  K. This discrepancy may be due to the role of the heat bath, i.e., the problem of dissipative LZS transitions (see, for example, [11] and references therein); however, a systematic investigation of this issue is in progress. More generally, it should be noted that, according to the above formula for  $t_{LZS}$ , it is the high sweep rates used in our experiment that ensure that the adiabatic LZS transitions take place over such a short time interval as to be clearly distinct from the hysteresis loops of the thermal relaxation regime.

The origin of LZS transitions in  $fV_6g$  remains to be discussed. The relatively large estimated value (0.4 K) of the zero-field energy gap for these molecules suggests that its origin cannot be due to dipolar or hyperfine fields. In addition, as explained above, the lowest energy levels of each independent triangle are doubly degenerate for  $B = 0$  (and not four-fold degenerate as in  $fV_{15}As_6g$  [8]) consistent with Kramers' theorem. Hence, for  $B = 0$  the ground state of such a molecule would consist of four degenerate states, namely the three symmetric states of the  $S = 1$  triplet and the antisymmetric  $S = 0$  singlet state. Inter-triangle exchange coupling could lift this degeneracy and give rise to avoided level crossings. However, since isotropic inter-triangle exchange cannot account for admixing states of total spin, we suggest that the avoided level crossings are due to the anisotropic (symmetric or antisymmetric) portion. One scenario is given in Fig. 1. The behavior of the dynamical magnetization thus involves LZS transitions between (at most) four levels. A detailed theoretical treatment of these transitions will be given elsewhere.

In summary, time-resolved magnetization measurements using sweep rates of order 1 Tesla/ms show hysteresis loops and magnetization steps for  $B = 0$  in the magnetic molecule  $fV_6g$ . The two effects are clearly distinct because of the relatively high sweep rates used in our experiment. In the absence of both an anisotropy energy barrier and the phonon bottleneck effect, the hysteresis effects exhibited by this molecule occur because the spin relaxation times are of the experimental

time scale. Using a generalization of the Bloch equation we were able to reproduce our experimental data for  $T = 1.7$  K and  $T = 4.2$  K for a large variety of field sweeps, and thus identify direct one-phonon resonant transitions among the Zeeman-split doublet of each triangle as the dominant mechanism underlying the hysteresis behavior. The main assumption of our model, namely that the phonons are in equilibrium with the cryostat, should break down for temperatures below 1 K due to the phonon bottleneck effect. In fact, our preliminary data at  $T = 0.6$  K indicate that the relaxation rate  $1/\tau$  deviates from Eq. (2). A systematic investigation of this issue is in progress. The steps of the magnetization for  $B = 0$  are attributed to adiabatic LZS transitions between lowest magnetic energy levels impacted by the existence of anisotropic inter-triangle exchange interaction of order 0.4 K. This estimate is consistent with that previously suggested by NMR data [1]. A more precise value of  $\Delta$  could possibly be determined by specific heat measurements [12], or by Electron Paramagnetic Resonance (EPR) techniques. The small departures from complete magnetization reversal suggests that one cannot entirely neglect the role of the heat bath. More generally, exploring nanomagnets with pulsed magnetic fields can reveal a variety of fascinating dynamical phenomena and provide microscopic information that otherwise is not readily accessible.

AMES Laboratory is operated for the U.S. Department of Energy by Iowa State University under Contract No. W-7405-Eng-82.

---

Electronic address: rusohatz@ameslab.gov

- [1] M. Luban et al, Phys. Rev. B 66, 054407 (2002).
- [2] L. Landau, Phys. Z. Sowjetunion 2, 46 (1932); C. Zener, Proc. R. Soc. London, Ser. A 137, 696 (1932); E. C. G. Stueckelberg, Helv. Phys. Acta 5, 369 (1932).
- [3] S. Miyashita, J. Phys. Soc. Jpn. 64, 3207 (1995).
- [4] A. Abragam and B. Bleaney, Electron Paramagnetic Resonance of Transition Ions (Clarendon Press, Oxford, 1970).
- [5] S. Miyashita, N. Nagaosa, Prog. Theor. Phys. 106, 533 (2001).
- [6] R. Sessoli, D. Gatteschi, A. Caneschi, and M. A. Novak, Nature (London) 365, 141 (1993).
- [7] C. Sangregorio et al, Phys. Rev. Lett. 78, 4645 (1997).
- [8] I. Chiorescu et al, Phys. Rev. Lett. 84, 3454 (2000); Phys. Rev. B 67, 020402(R) (2003).
- [9] F. Bloch, Phys. Rev. 70, 460 (1946); 102, 104 (1956); 105, 1206 (1957).
- [10] I. Rouschatzakis and M. Luban (unpublished)
- [11] M. Nishino, K. Saito and S. Miyashita, Phys. Rev. B 65, 014403 (2001).
- [12] M. A. Roncete et al, Phys. Rev. Lett. 88, 167201 (2002); Phys. Rev. B 68, 104403 (2003).
- [13] We anticipate that a similar relation holds for the general 4-level LZS problem.